

List of Supplementary Materials

Extended fig. 1 to 12

Extended figure 1: Psychophysics of the response of PIEZO2^{DS} individuals for the hair being pulled in the arm and leg.

Extended figure 2: Pain qualities in response to pinprick and hair-pull stimulation.

Extended figure 3: Quantifying skin mechanics for hair-pull and indentation.

Extended Figure 4: Functional characterization of hair-pull responses in non-specific Piezo2cKO.

Extended Figure 5: Molecular profiling of Trpm8^{low} neurons.

Extended figure 6: Trpm8:iCre line faithfully targeted all Trpm8 expressing neurons.

Extended figure 7: Postnatal labelling of Trpm8:iCre neurons using AAV/PHP.S serotype targets exclusively Trpm8^{low} cells.

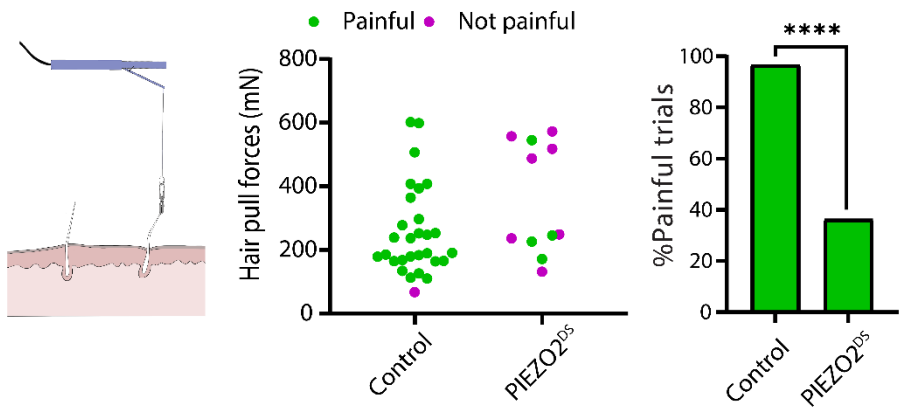
Extended figure 8: Functional characterization of hair pull responses in transgenic models.

Extended figure 9: Receptive field locations.

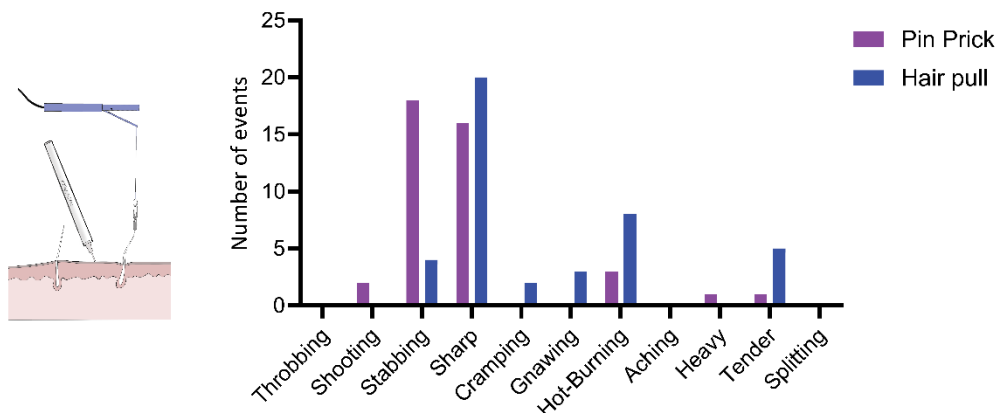
Extended figure 10: Hair-pull pain is not mediated by LTMRs.

Extended figure 11: Hair-pull pain is not mediated by LTMRs or cooling-unresponsive A-HTMRs.

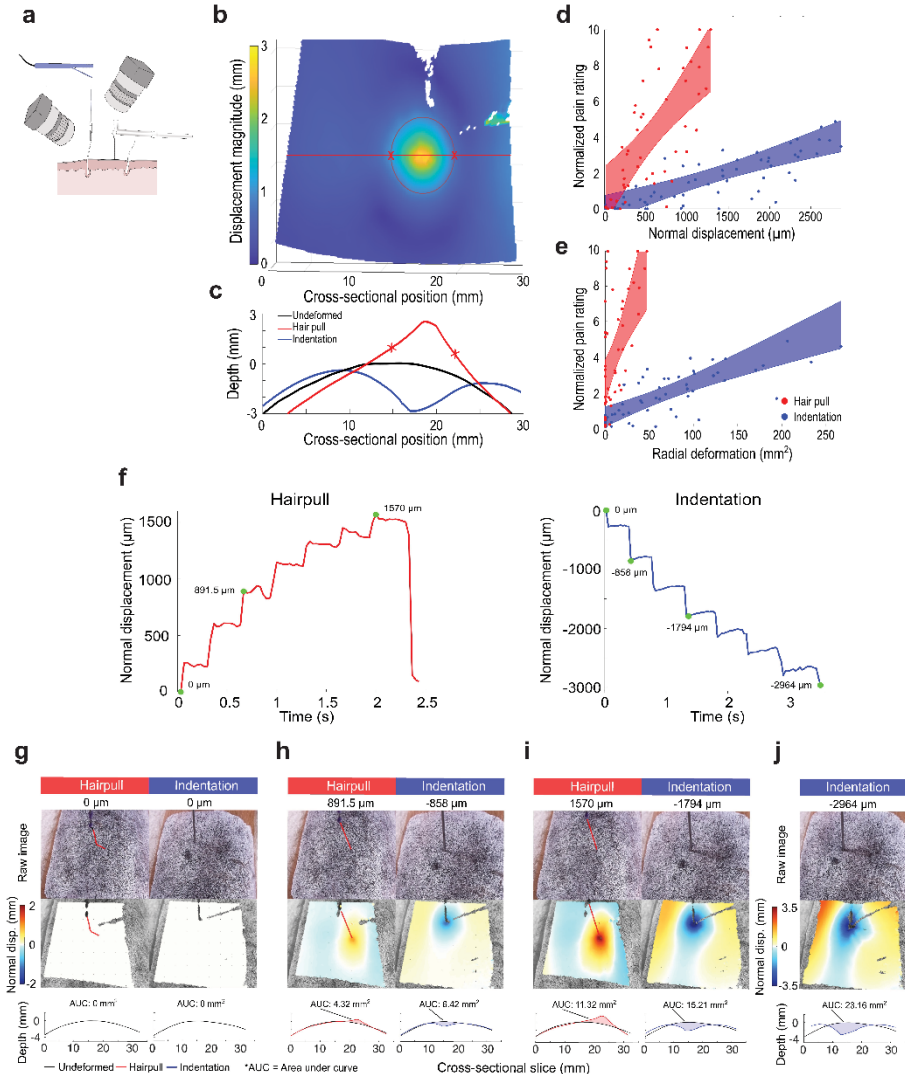
Extended figure 12: Somatosensory testing to monitor nerve block progression.



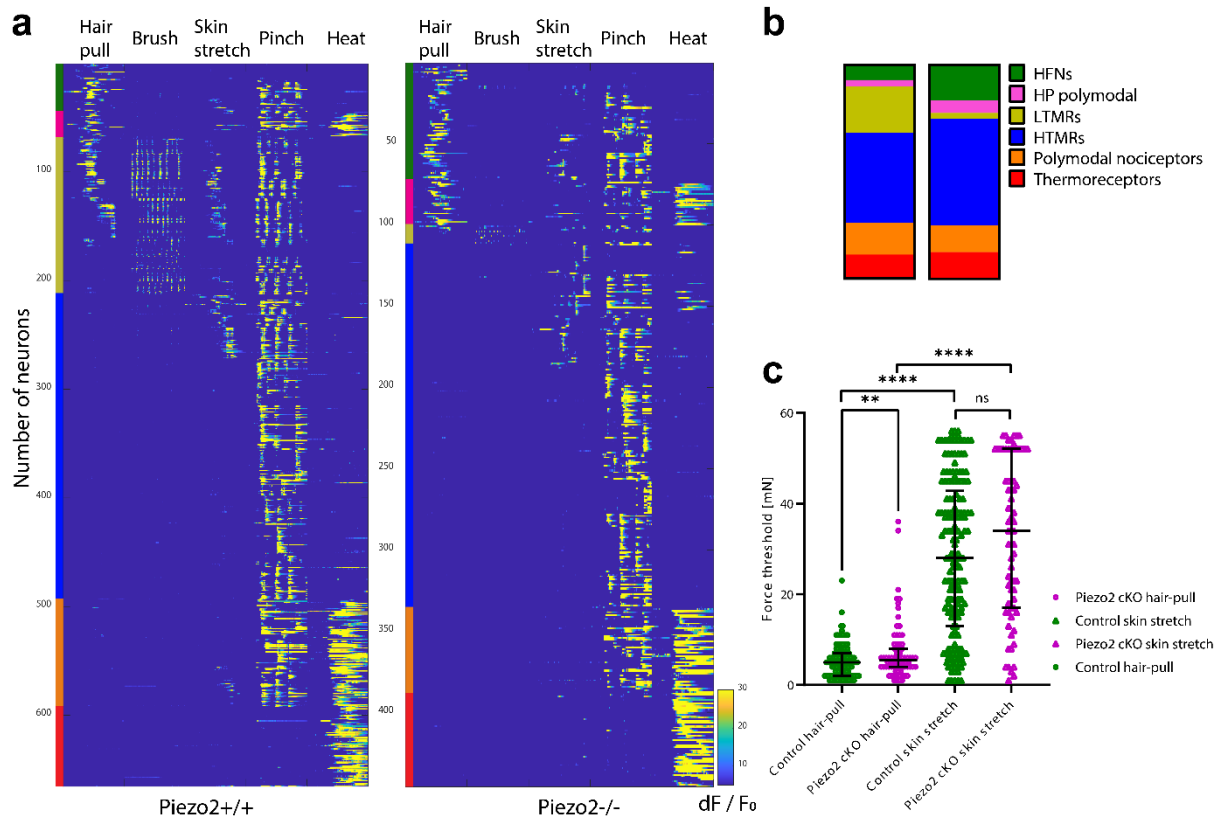
Extended figure 1: Psychophysics of the response of PIEZO2^{ds} individuals for the hair being pulled in the arm and leg. Similarly to scalp hair, pulling of forearm and leg hair evoked pain in control subjects (n=7), but PIEZO2^{ds} individuals (n=6) reported the pain to be significantly diminished or non-existent. At similar pulling forces, most hair pulling trials were reported as non-painful by PIEZO2^{ds} subjects. Dots represent individual trials (control participants: n=29 trials, PIEZO2^{ds} individuals: n=11 trials). The histograms represent the percentage of trials reported as painful (control participants: 96.7% vs. PIEZO2^{ds} individuals: 36.4%, p<0.0001; Fisher's exact test).



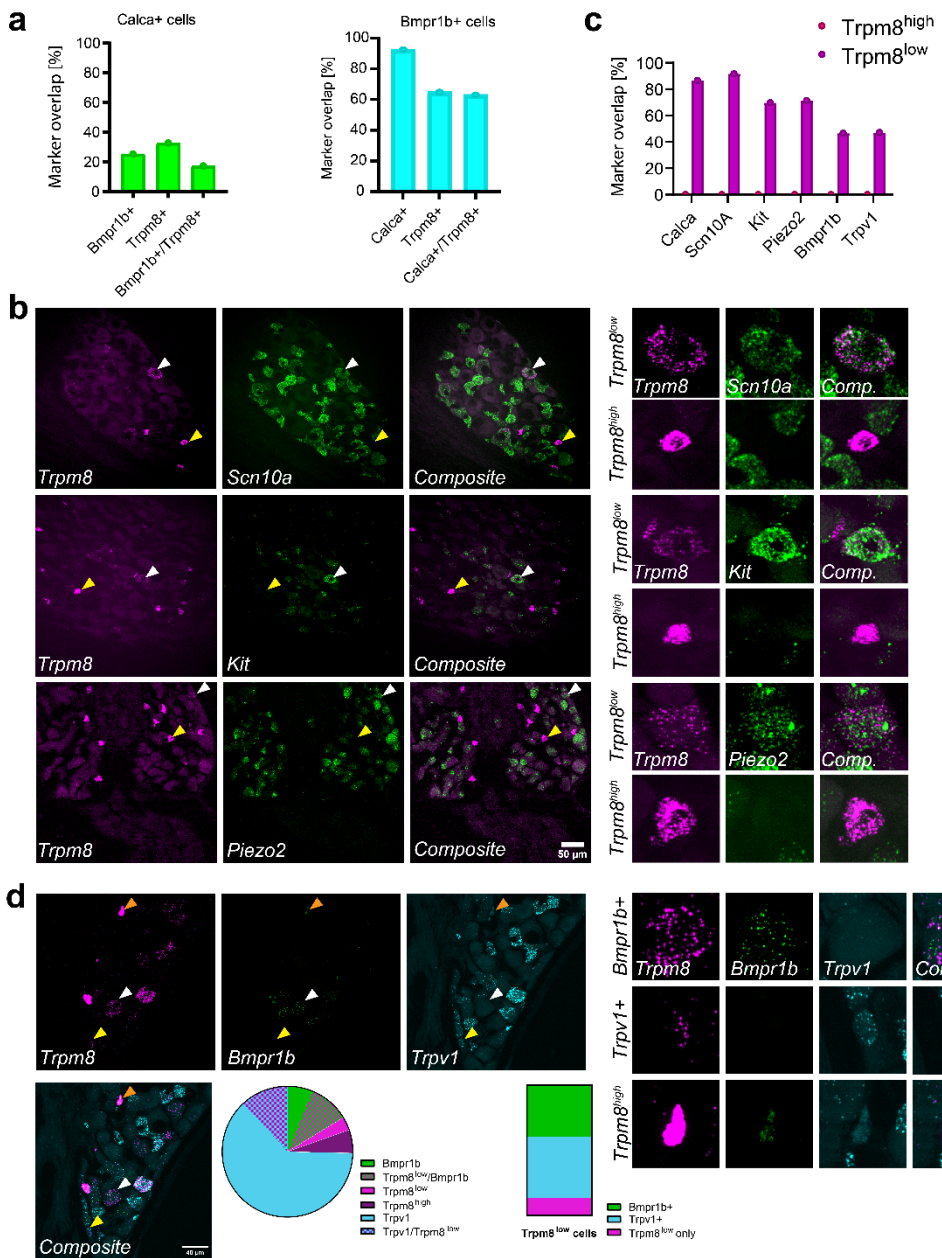
Extended figure 2: Pain qualities in response to pinprick and hair-pull stimulation. McGill pain quality data in response to hair-pulling and pinprick stimulation at equivalent pain intensities. The data, collected from 5 healthy participants, show the number of occurrences (events) for each pain descriptor, including common descriptors ('sharp') and those preferentially chosen for pinprick pain ('stabbing') and hair-pull pain ('hot-burning' and 'tender').

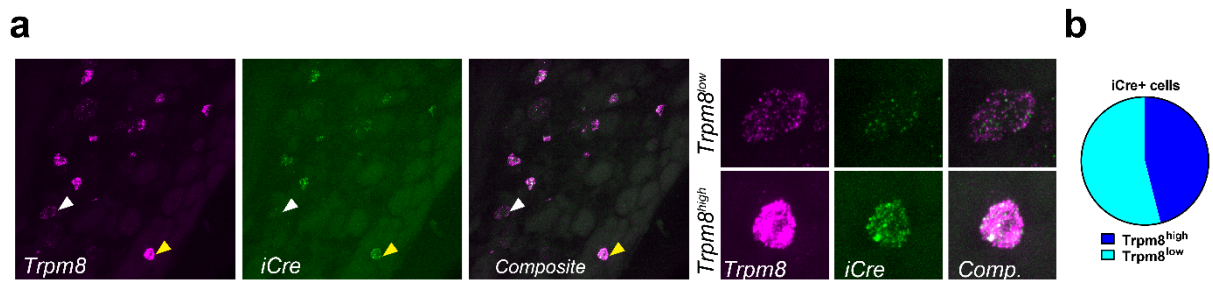


Extended figure 3: Quantifying skin mechanics for hair-pull and indentation. **a.** Comparing states of skin deformation between hair pull and normal indentation using 3D digital image correlation. **b.** 3D point cloud showing the change in skin surface displacement from the initial state during hair pull on the forearm ($t=0 \rightarrow t=33$ sec). Yellow color depicts greater movement in the x, y, and z directions as compared to purple color depicting no change from the undeformed state. Displacement increases radially inward towards the point of hair pull. The red line marks the central cross-section of the 3D surface, taken at each time point to visualize the normal deformation of the skin surface. From the 3D point cloud, the field of points displacing more than 1 mm are fitted with a 2D ellipse, depicted by the red ring. To quantify lateral deformation, radial deformation is measured as the area of this ellipse. **c.** The undeformed cross-section before contact (black, $t=0$ s), at maximum deformation during the same hair pull trial (red, $t=33$ s), and at matching depth during a normal indentation trial (blue, $t=12.7$ s). Similar deformation patterns are exhibited between hair pull and normal indentation, while hair pull extends the skin above the undeformed surface and indentation deforms the skin below the undeformed surface. **d.** Aggregate raw data of normal displacement for all trials and all participants fit with a linear line and shaded regions depicting the 95% confidence intervals. Higher normalized pain levels are reported at similar levels of normal displacement for hair pull as compared to normal indentation. **e.** Radial deformation plotted by normalized pain rating showing a steeper slope for hair pull pain as compared to normal indentation pain, despite similar levels of radial deformation, or lateral skin surface movement. Data are represented as average \pm SEM. Dots showed the individual trials. **f.** Raw trace of skin normal displacement over time for one hair pull trial (red) and one indentation trial (blue). Green dots mark the time points visualized in panels **g-j** below. A maximum normal displacement of 1570 μ m is measured during the hair pull trial while a maximum of -2964 μ m is measured during indentation, indicating that greater skin deformation can be reached in indentation trials, as compared to hair pull trials, before pain thresholds are reached. **g.** The raw speckled image, normal displacement, and cross-sectional slice for the same hair pull trial and indentation trial as **(b)** taken at $t = 0$ sec, or normal displacement = 0 μ m, for the same participant. No difference in initial states was observed and the area under the curve (AUC) was 0 mm^2 for both trials. **h.** At similar steps of normal displacement (hair pull: 891.5 μ m, indentation: -858 μ m), similar, though inverted, fields of normal displacement and cross-sectional slices were observed. While orange color depicts upward movement for hair pull, and blue color depicts downward movement for indentation, the magnitudes of normal displacement were similar at these two points. Similarly, the cross-sectional slices maintained similar curvature and AUC measurements. **i.** A further step in normal displacement depicted increasing deformation for both trials, while maintaining similarities in deformation pattern and AUC measurements. **j.** A final step in indentation, unmatched by hair pull, reinforced how indentation trials can reach greater states of deformation before reaching pain thresholds, as compared to hair pull trials.

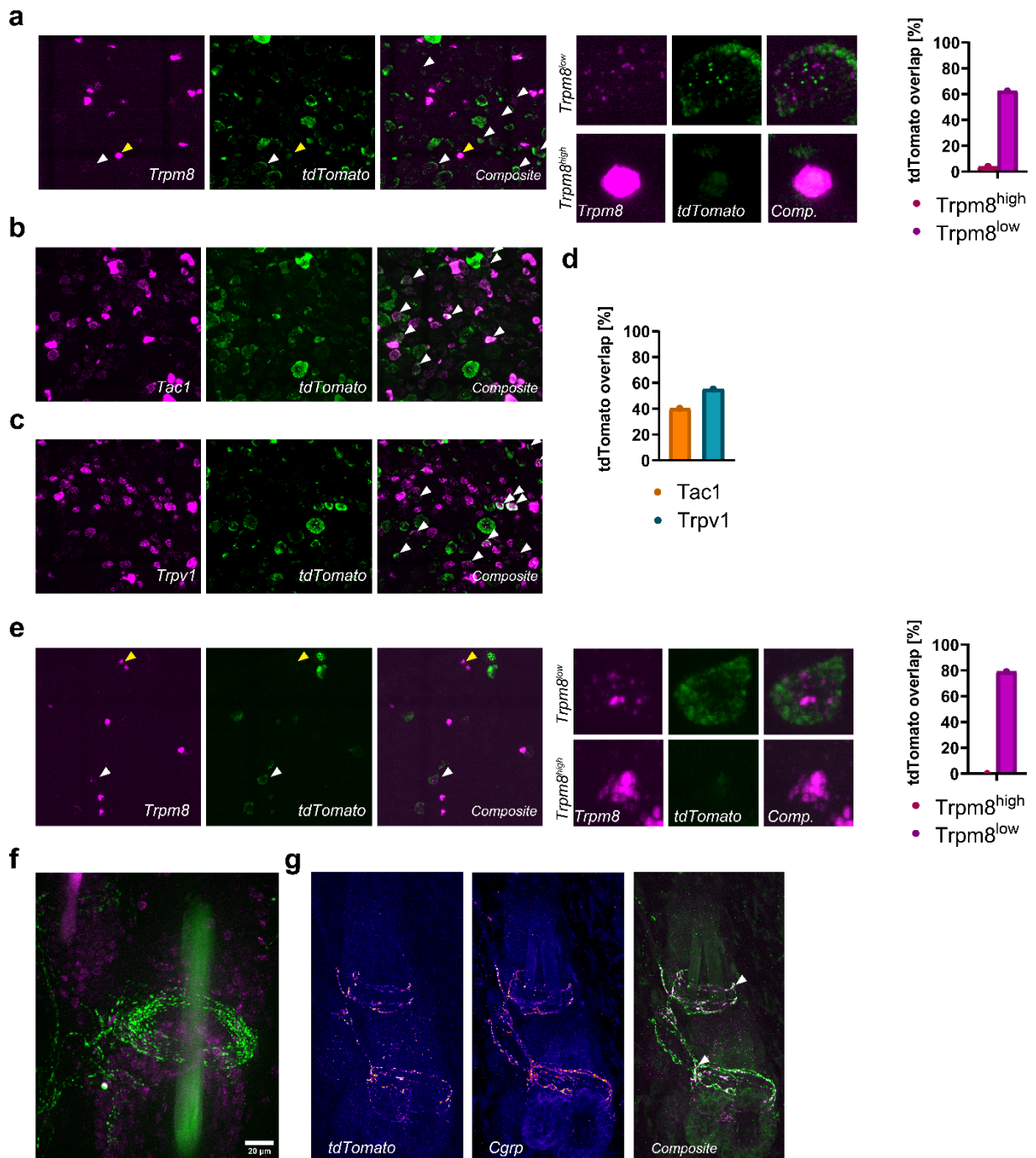


Extended figure 4: Functional characterization of hair-pull responses in non-specific Piezo2cKO. **a-b.** To distinguish the neuron populations responsible for hair pulling, we applied gentle brush, skin stretch (pulling the hair with a thread glued to depilated skin, imitating skin deformation upon hair pulling), pinching, and heating to regions of the cheek and recorded calcium responses in the trigeminal ganglia. We found that hair pulling triggered activation of three categories of mechanosensory afferents. The first group responded preferentially to hair pull and pinching (hair pull responsive mechanoreceptors 7%), matching the functional characteristics of Calca+ Trpv1- nociceptors that we identified previously as A-type high threshold mechanoreceptors (Ghitani et al. 2017). The second group responded to high threshold mechanical stimuli and noxious temperature (HP Polymodal nociceptors 3.2%). The third group (LTMRs 21.5%) always responded to brushing and reacted to high threshold stimuli such as pinching but not heat application. This indicates that those neurons relied on force transduction within the hair follicle to tune their sensitivity similarly to our observations in human subjects. Loss of Piezo2 led to complete loss of response to stroking (LTMRs 2%), congruent with previous reports (Szczot et al. 2018, von Buchholtz et al. 2021). The proportion of neurons responding to single hair pull in mosaic Piezo2 KO animals was higher than in controls (hair pull responsive mechanoreceptors 16.6%). **c.** Lack of Piezo2 heightened the activation threshold for hair-pull responsive neurons. Skin stretches activated neurons at forces orders of magnitude higher than those needed to pluck out the hair, but Piezo2 knock-out did not affect the activation threshold.

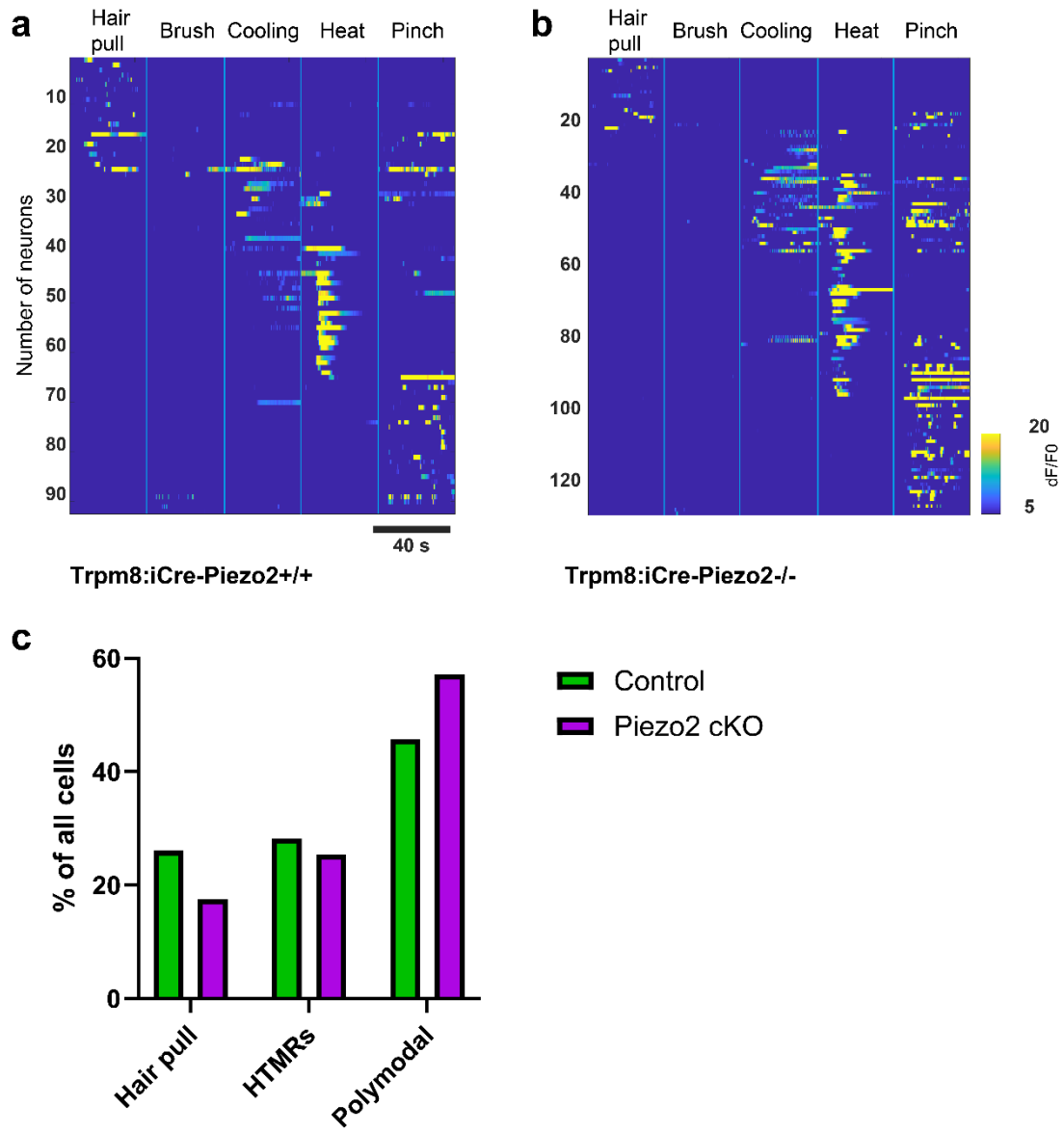




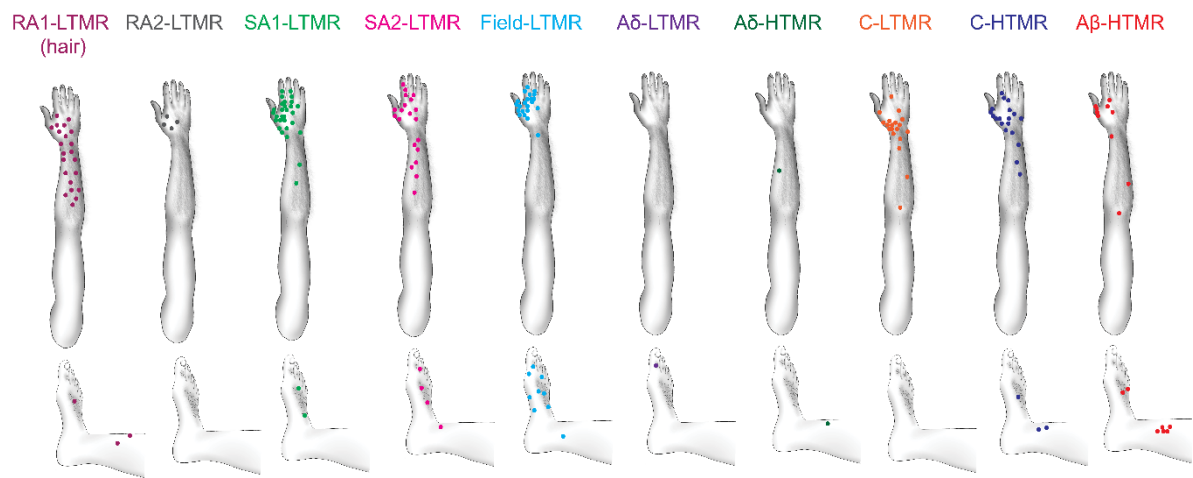
Extended figure 6: $Trpm8:iCre$ line faithfully targeted all $Trpm8$ expressing neurons. **a.** Fluorescence *in situ* hybridization confirms that $Trpm8:iCre$ faithfully targeted both $Trpm8^{low}$ and $Trpm8^{high}$ cells. White and yellow arrows point to $Trpm8^{low}$ and $Trpm8^{high}$ cells respectively, zoomed in on the right. **b.** Quantification of FISH data showing the proportion of labelled $Trpm8^{low}$ and $Trpm8^{high}$ DRG cells.



Extended figure 7: Postnatal labelling of *Trpm8* neurons using AAV/PHP.S serotype targets exclusively *Trpm8*^{low} cells. **a.** FISH images of wild-type murine DRG neurons targeted by postnatally injected Cre-independent AAV/PHP.S-CAG-tdTomato show co-expression of tdTomato and *Trpm8* mRNA only in *Trpm8*^{low} cells. Yellow arrow marks a *Trpm8*^{high} cell and white arrows point to examples of *Trpm8*^{low} cells colocalizing with tdTomato. **b-d.** tdTomato expressing neurons show a significant overlap with *Tac1* and *Trpv1* genes. **e.** FISH of DRG neurons labelled with Cre-dependent AAV/PHP.S-CAG-LSL-tdTomato showed expression of tdTomato in *Trpm8*^{low} but not *Trpm8*^{high} cells. **f.** *Trpm8*:iCre efficiently labelled circumferential endings in mouse hairy back skin. *Trpm8*:iCre animals were postnatally injected with cre dependent reporter (AAV/PHP.S-CAG-LSL-tdTomato). tdTomato in green and DAPI in magenta. **g.** Immunostaining of hairy skin of TRPM8:iCre mice postnatally labelled with AAV/PHP.S-CAG-LSL-tdTomato showed hair follicle associated nerve endings co-expressing tdTomato and CGRP (green and magenta respectively in the composite panel). Orange arrows point to colocalization hot spots.



Extended figure 8: Functional characterization of hair pull responses in transgenic models. **a-b.** Heatmaps of neuronal activity of murine control (a) and Piezo2 cKO (b) sensory neurons delineated by $Trpm8^{iCre}Rosa26^{LSLGCaMP6f}$ genetic model with postnatal labelling by AAV/PHP.S-CAG-LSL-mNeptune virus. Only neurons showing GCaMP signals and mNeptune fluorescence were analyzed. **c.** Percentages of functional populations of $TRPM8^{iCre}$ neurons with and without Piezo2. Neurons responding to hair pull were ascribed to HFN category. Cells responding only to pinching were classified as HTMRs. Temperature responsive cells were classified as polymodal.

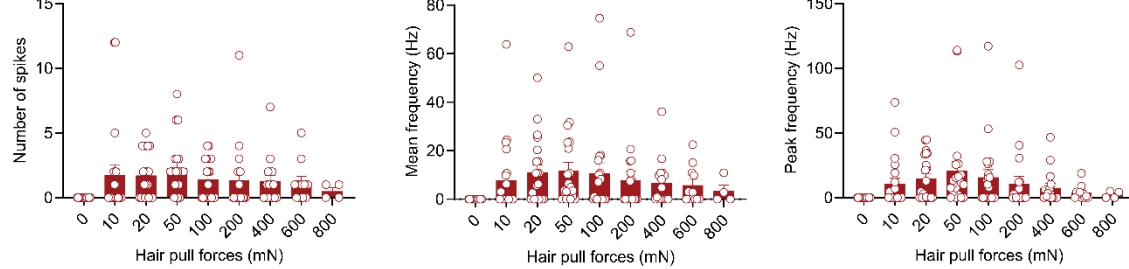


Extended figure 9: Receptive field locations. Locations of all afferent types from recordings in the peroneal, antebrachial, and radial nerves, with each dot representing an individual afferent (n=180).

a RA1-LTMR (hair)

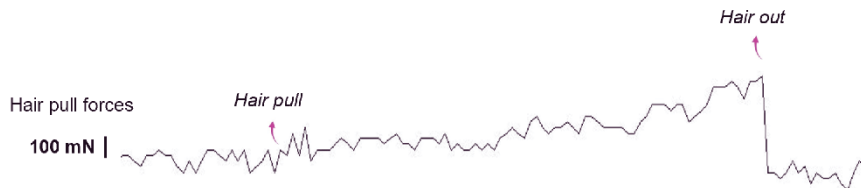


b

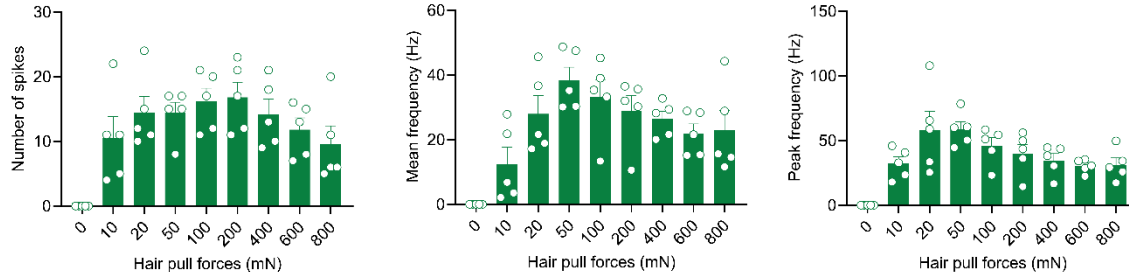


c

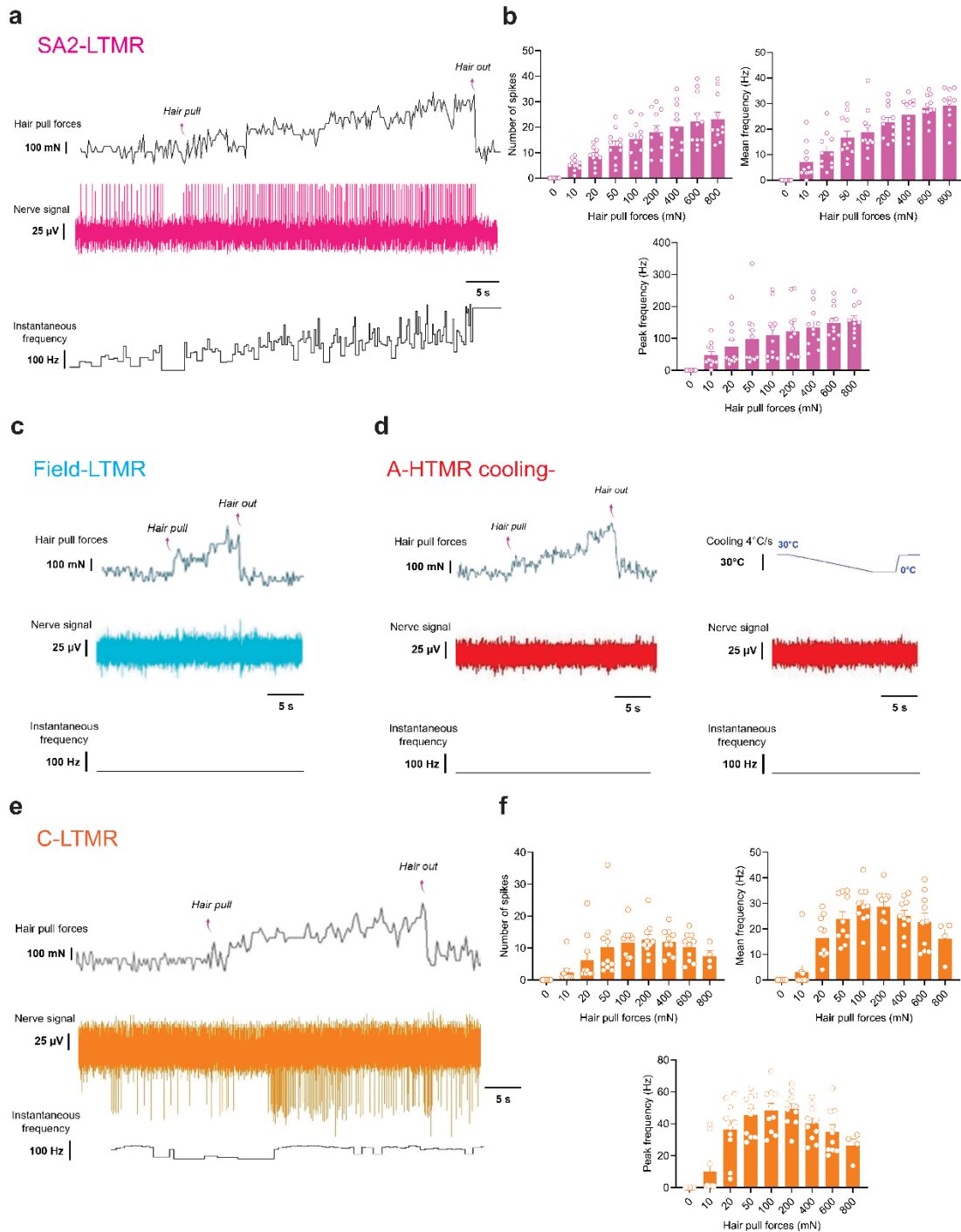
SA1-LTMR



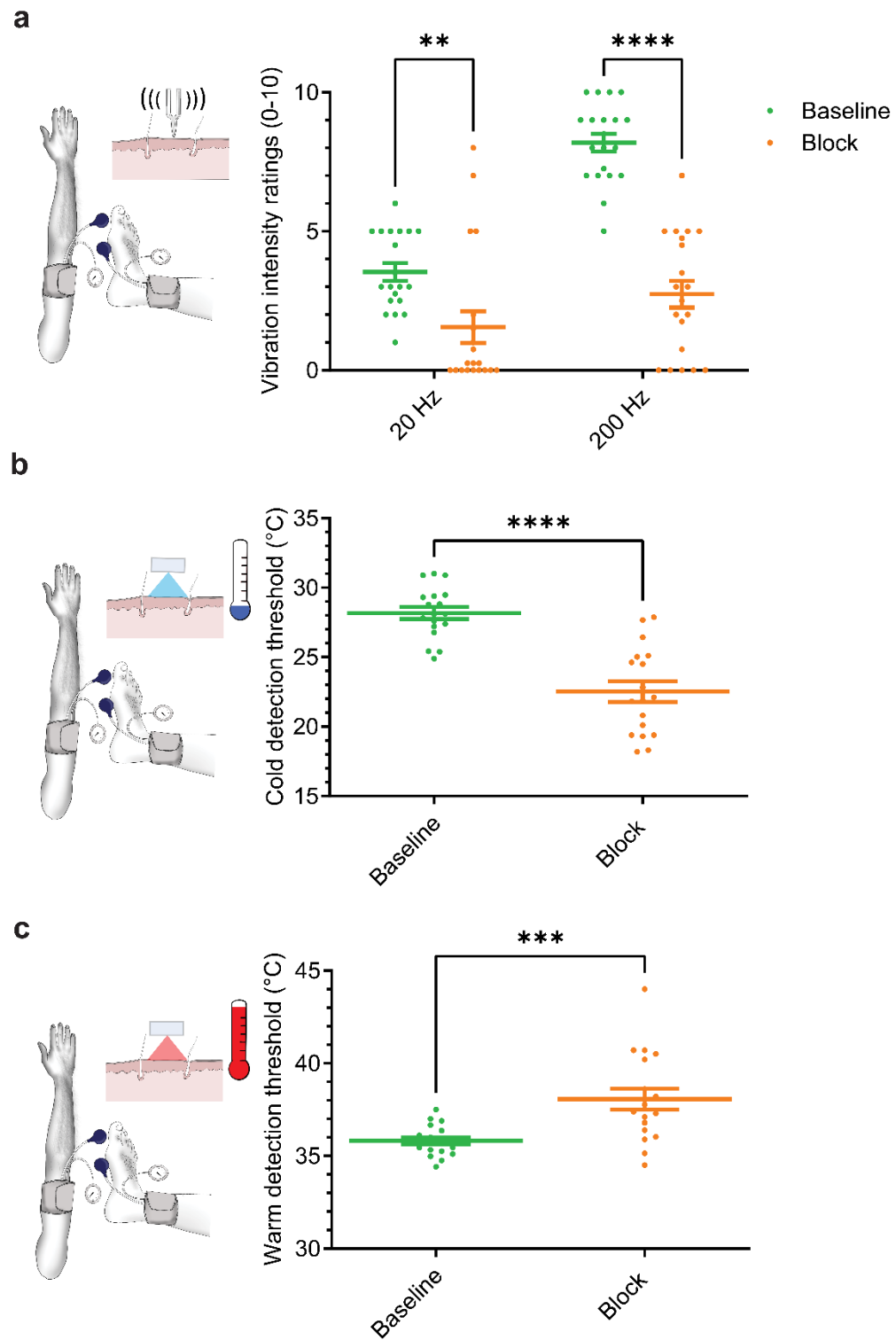
d



Extended figure 10: Hair-pull pain and responses from LTMRs. **a.** Representative neural trace showing response of an RA1-LTMR to a single hair-pull. **b.** Neural discharge (number of spikes and mean and peak frequencies) of RA1-LTMRs (n=13 units). Hair pulling forces had no significant effect on the number of spikes ($F_{(10,168)} = 1.861$, $p=0.0538$), mean frequency ($F_{(10,168)} = 1.54$, $p=0.1281$), or peak frequency ($F_{(10,168)} = 2.13$, $p=0.0245$). The data show individual trials and mean (\pm SEM) responses of RA1-LTMRs (n=19 trials) to hair pulling at different forces. **c.** Representative neural trace showing response of an SA1-LTMR to a single hair-pull. **d.** Neural discharge (number of spikes and mean and peak frequencies) of SA1-LTMRs (n=5 units). Hair pulling forces had no significant effect on the number of spikes ($F_{(10,44)} = 8.35$, $p=0.2855$), mean frequency ($F_{(10,44)} = 8.44$, $p=0.3269$), or peak frequency ($F_{(10,44)} = 9.64$, $p=0.0321$). The data show individual trials and mean (\pm SEM) responses of SA1-LTMRs to hair pulling at different forces. Statistical differences were assessed using one-way ANOVA with Tukey's multiple comparisons test.



Extended figure 11: Hair-pull pain and responses from LTMRs or cooling-unresponsive A-HTMRs. **a.** Representative neural trace showing response of an SA2-LTMR to a single hair-pull. **b.** Neural discharge (number of spikes and mean and peak frequencies) of SA2-LTMRs ($n=7$ units). Most SA2s were spontaneously active. Hair pulling forces had a significant effect on the number of spikes ($F_{(10,109)} = 18.05$, $p<0.0001$), as well as on the mean ($F_{(10,109)} = 35.52$, $p<0.0001$) and peak frequencies ($F_{(10,109)} = 9.97$, $p<0.0001$). No significant differences were found in the peak frequencies between 800 mN and all forces tested ($p>0.05$). The data show individual trials and mean (\pm SEM) responses of SA2-LTMRs ($n=11$ trials) to hair-pull at different forces. **c.** Representative neural trace of a field-LTMR to a single hair-pull. All field-LTMRs ($n=5$ units) were unresponsive to hair-pull. **d.** Representative neural traces of a cooling-unresponsive A-HTMR to single hair-pull and cooling. All A-HTMR cooling- ($n=7$ units) were unresponsive to hair-pull. The mechanical threshold, conduction velocity and cooling response of five A β -HTMRs from this sample were previously published in a preprint (Yu et al., 2024). **e.** Representative neural trace showing response of a C-LTMR to a single hair-pull. **f.** Neural discharge (number of spikes and mean and peak frequencies) of C-LTMRs ($n=10$ units). Hair pulling forces had a significant effect on the number of spikes ($F_{(7,72)} = 7.04$, $p<0.0001$), as well as on the mean ($F_{(7,72)} = 20.21$, $p<0.0001$) and peak frequencies ($F_{(7,72)} = 19.89$, $p<0.0001$). However, no significant effect was seen in the peak frequencies between 800 mN and all forces tested ($p>0.05$). The data show individual and mean (\pm SEM) responses of C-LTMRs to hair-pull at different forces. Statistical differences were assessed using one-way ANOVA with Tukey's multiple comparisons test.



Extended figure 12: Somatosensory testing to monitor nerve block progression. **a.** Vibration intensity task. Vibration intensity ratings in response to low (20 Hz) and high (200 Hz) frequencies at 'Baseline' and during preferential ischemic 'Block' of A β fibers. The vibration intensity ratings significantly decreased ($F_{(1,19)} = 43.85$, $p<0.0001$) during the block for both frequencies (Baseline vs. Block: [20 Hz]: $t=3.72$, $p<0.001$ and [200 Hz]: $t=10.22$, $p<0.0001$). The data show individual- and pooled-mean (\pm SEM) vibration intensity ratings (tested in triplicate; $n=20$ participants). Statistical differences were assessed using one-way ANOVA with Tukey's multiple comparisons test. **b.** Cold detection threshold. Nonpainful cooling sensitivity decreased significantly during the block (Baseline vs. Block: $t=6.23$, $p<0.0001$; Paired t-test). Nonetheless, all participants retained the ability to detect cold in the non-painful range (cold pain $<10^{\circ}\text{C}$). The data show individual- and pooled-mean (\pm SEM) cold detection thresholds (tested in triplicate; $n=20$ participants). **c.** Warm detection threshold. Nonpainful warming sensitivity decreased significantly during the block (Baseline vs. Block: $t=4.27$, $p=0.0005$; Paired t-test). Nonetheless, all participants retained the ability to detect warmth in the non-painful range (heat pain $>40^{\circ}\text{C}$). The data show individual- and pooled-mean (\pm SEM) warm detection thresholds (tested in triplicate; $n=20$ participants).